aerospace

MDPI

Article

Performance Comparison of Control Strategies for a Variable-Thrust Solid-Propellant Rocket Motor

Jihyoung Cha [1,*] and Élcio Jeronimo de Oliveira [1,2]

[1] Department of Computer Science, Electrical and Space Engineering, Luleå University of Technology, RYMDCAMPUS 1, 98192 Kiruna, Sweden; elcioejo@innospc.com.br
[2] INNOSPACE Brazil, Av. São João 2375, São José dos Campos 12242-000, Brazil
* Correspondence: jihyoung.cha@ltu.se

Abstract: This paper deals with a performance comparison of the control algorithm for a variable-thrust solid-propellant rocket motor (VTSRM). To do this, we develop a simulation model of a VTSRM considering characteristic changes in the combustor and design control systems for pressure and thrust. We use three types of control algorithms for the pressure control: classical PID control, feedback linearization control, and fuzzy PID control, and two control algorithms for thrust control: classical PID control and fuzzy PID control. Finally, we compare the performance of each control system through a numerical simulation using step responses. Through this work, we check that feedback linearization is better in pressure control, and fuzzy PID control is more appropriate in thrust control. Especially using fuzzy PID control, we can get fast settling with a small undershoot even if the system is a nonminimum phase system.

Keywords: variable-thrust solid-propellant rocket motor; pressure control; thrust control; nonminimum phase system; performance comparison

check for updates

Citation: Cha, J.; de Oliveira, É.J. Performance Comparison of Control Strategies for a Variable-Thrust Solid-Propellant Rocket Motor. *Aerospace* **2022**, *9*, 325. https://doi.org/10.3390/aerospace9060325

Academic Editors: Mikhail Ovchinnikov and Dmitry Roldugin

Received: 20 May 2022
Accepted: 11 June 2022
Published: 16 June 2022

Publisher's Note: MDPI stays neutral with regard to jurisdictional claims in published maps and institutional affiliations.

Copyright: © 2022 by the authors. Licensee MDPI, Basel, Switzerland. This article is an open access article distributed under the terms and conditions of the Creative Commons Attribution (CC BY) license (https://creativecommons.org/licenses/by/4.0/).

1. Introduction

Solid-propellant rocket motors (SRMs) have simple structures and are suitable for long-term storage compared to other types of propellant systems, so they have been used for various applications [1–5]. However, once the specifications of an SRM, including propellant and nozzle throat area, are determined, the thrust level of the system is generally fixed and hard to control [1]. In the recent two or three decades, to overcome the weakness of the system, the studies related to a variable-thrust solid-propellant rocket motor (VTSRM) using the special nozzle with a pintle valve have been progressed [6,7]. The pintle nozzle is a special nozzle with a movable pintle to change the nozzle throat area. It causes chamber pressure and nozzle exit pressure to be adjusted, so the thrust control becomes available by the effects, as shown in Figure 1.

Furthermore, these days, using these characteristics, the ramjet or scramjet system, called dual-mode ramjet (DMRJ) or solid-fuel rocket scramjet (SFRSCRJ), has been developed and studied as in Figure 2 [8–11]. The fuel-rich combustion gas, generated from the solid propellant system, is controlled by the pintle, and it makes variable thrust in the ram combustor. Therefore, the characteristics of the system drive are one of several challenges in the DMRJ, and SFRSCRJ is the accurate control of combustion gas flow rate using a control valve such as a pintle valve.

However, although pressure or thrust will be controlled by a pintle accurately and straightforwardly, there is a limited position to move the pintle, as shown in Figure 3. If a pintle moves closer to the nozzle throat pass over the limited position, a severe accident can occur, such as an explosion, because of the unbalance of pressure and exit mass flow rate. Therefore, the pressure and thrust control by appropriate pintle position with stability is the main subject for single-nozzle VTSRPM and thrust distribution by pintle position for the multi-nozzle with stable pressure. For the design control system, a dynamic simulation model of a VTSRM is required, and modeled as a nonlinear differential equation with

respect to the nozzle throat area, pressure, and other system variables. However, there are also uncertainties in system parameters, such as solid fuel regression and discharge coefficient [12]. Therefore, for effective pressure and thrust control of a VTSRM, it is essential to design the control algorithms considering the nonlinearity and uncertainty [13].

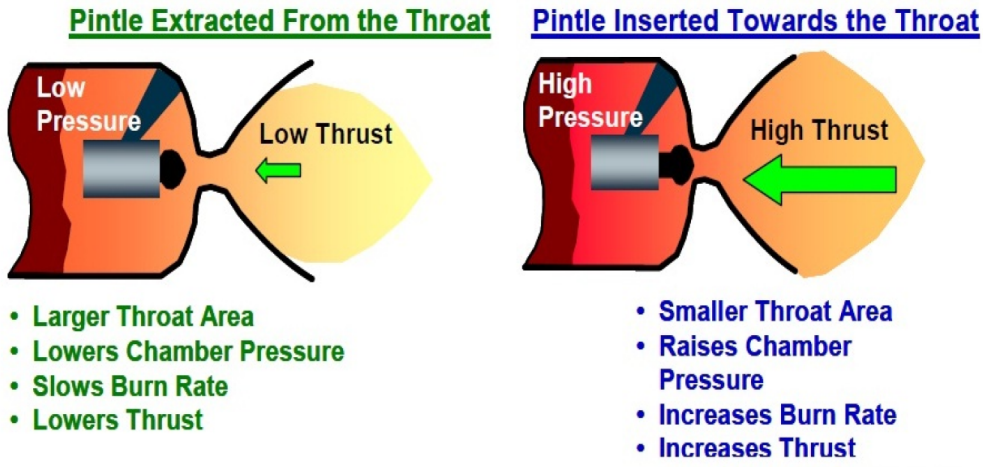

Figure 1. Pintle nozzle technology to control thrust by chamber pressure andthroat area [7].

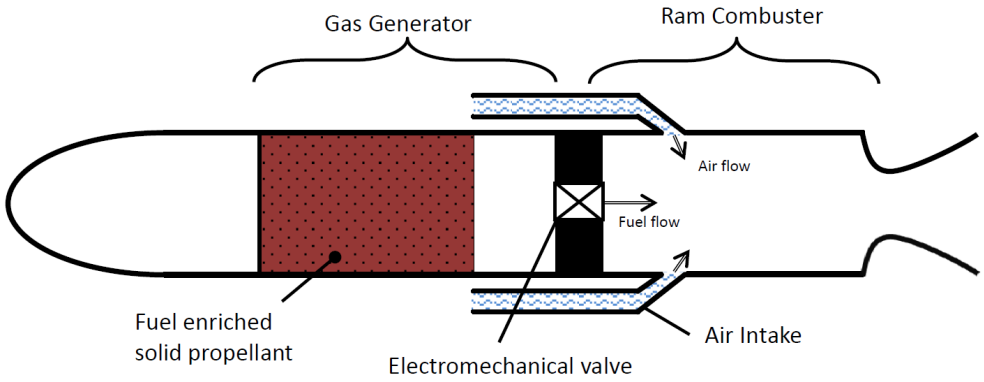

Figure 2. Schematic of throttleableducted rocket [8].

For these reasons, many studies have been carried out to solve the issues keeping these advantages of VTSRM, focusing on several concepts: control of thrust and combustion pressure [13–16], a reaction control system (RCS) composed of multiple nozzles for divert and attitude control [17–20], the flow characteristics by pintle shape using computational fluid dynamics (CFD) [21–24], the experiment using cold or hot gas [25,26], and a part of ramjet or scramjet to generate and control the fuel-rich combustion gas [8–11].

The most famous control algorithm is the classical PID control because it has a simple structure and robust performance in a wide range of operating conditions. However, the control is not suitable for a strongly nonlinear system with uncertainties. Therefore, two nonlinear control algorithms are used for VTSRM: feedback linearization and fuzzy PID control. Feedback linearization is one of the robust nonlinear control algorithms used in various areas, including aerospace and control fields [27,28]. However, the feedback linearization has essential drawbacks in the uncertain system and external disturbance [29]. Fuzzy PID control has been widely used for industrial processes owing to its heuristic nature associated with simplicity and effectiveness for linear and nonlinear systems. Since the method is robust and proven in many fields, it has been applied to various aerospace systems [30–32].

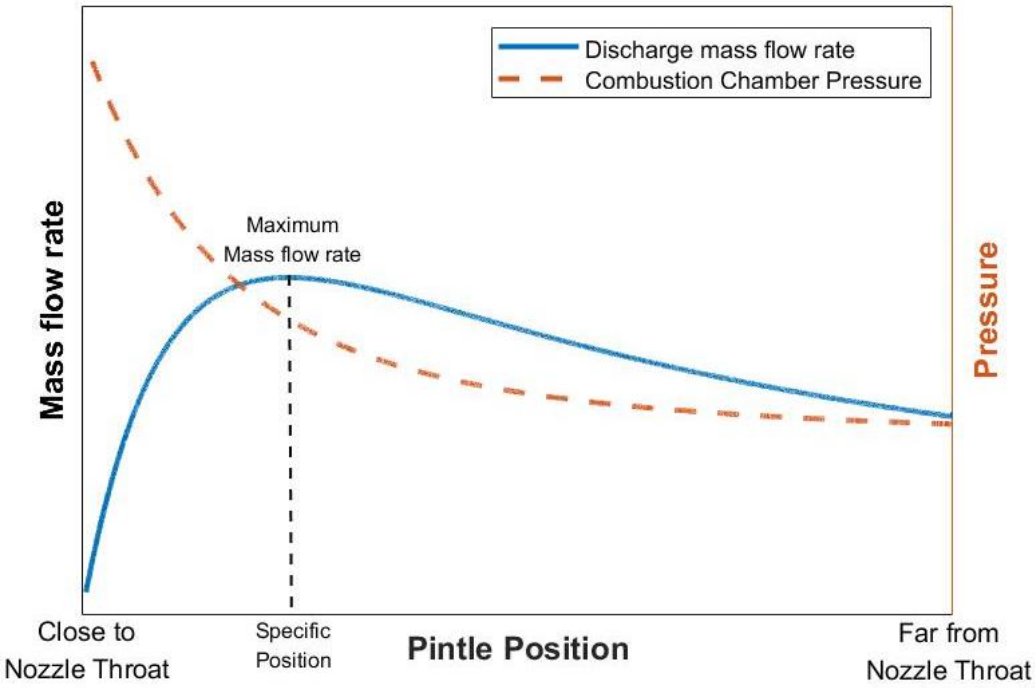

Figure 3. Discharge mass flow rate and pressure based on pintle position of single-nozzle system.

However, it is hard to find research related to the nonlinear control algorithm for VTSRM and its performance. Therefore, this study aims to design and compare the performance of the control algorithm for a VTSRM pressure and thrust with a single nozzle. To compare the control algorithm, we design and compare the performance of three types of pressure control and two types of thrust control. To do this, we first develop a mathematical model of a VTSRM considering characteristic changes in the combustor. After that, we design several controllers, including classical PID control and nonlinear control, which are feedback linearization and fuzzy PID control, for pressure and thrust. Finally, we conduct a simulation and compare each control performance using step input. The following section briefly introduces the dynamic simulation model of a VTSRM considering characteristic changes in the combustor. Then, Sections 3 and 4 explain the control algorithm for pressure and thrust, respectively. Section 5 analyzes and compares the performance of each control algorithm. Finally, Section 6 concludes the study.

2. Mathematical Modeling

2.1. Solid-Propellant Rocket Motor Specification

For the governing equations of VTSRM behavior, the schematic of a VTSRM with pintle nozzle is shown in Figure 4. In the figure, the solid propellant shape is simplified as an end-burning type, and the mass balance in the free volume will be discussed as a driving mechanism of the combustion pressure according to the pintle movement.

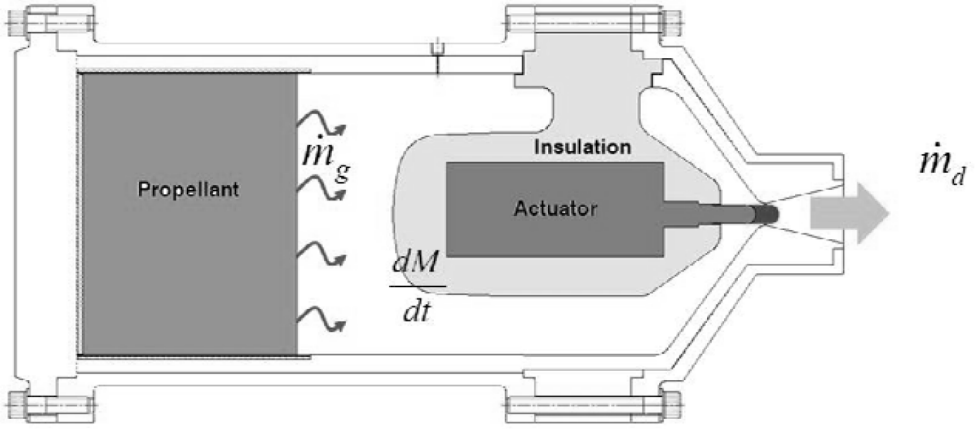

Figure 4. Schematic of variable-thrust solid-propellant rocketmotor with pintle nozzle [33].

2.2. Pressure Dynamic Modeling

According to the physical model presented in Figure 4, the mass generated from the solid propellant surface should be balanced with the mass flow rate through the nozzle, and the mass accumulated in the free volume is expressed as the following equation:

$$\dot{m}_g = \frac{dM}{dt} + \dot{m}_d \tag{1}$$

The first term on the right-hand side in Equation (1) represents the accumulated mass and can be calculated by the following equation:

$$\frac{dM}{dt} = \frac{d}{dt}(\rho_c V_{fv}) = \rho_c \frac{dV_{fv}}{dt} + V_{fv} \frac{d\rho_c}{dP_c} \frac{dP_c}{dt} \tag{2}$$

$$\frac{dP_c}{d\rho_c} = c^2 = kRT \tag{3}$$

Assuming the system is adiabatic and using the state equations, the combustion pressure can be described using the following equation:

$$\frac{dP_c}{dt} = \frac{c^2}{V_{fv}} \left(\dot{m}_g - \dot{m}_d - \rho_c \frac{dV_{fv}}{dt} \right) \tag{4}$$

Assuming no erosive burning, the mass generation rate at the solid propellant surface and the discharged mass flow rate through the nozzle exit can be expressed as follows [34]:

$$\dot{m}_g = \rho_p A_b a P_c^n \tag{5}$$

$$\dot{m}_d = A_t P_c \sqrt{\frac{k}{RT}} \left(\frac{2}{k+1} \right)^{(k+1)/[2(k-1)]} = \frac{P_c A_t}{C^*} \tag{6}$$

$$C^* = \sqrt{\frac{RT}{k} \left(\frac{k+1}{2} \right)^{\frac{k+1}{k-1}}} \tag{7}$$

Assuming the free volume change is related only to the propellant surface movement due to propellant burning, the time rate of the free volume change is expressed as follows:

$$\frac{dV_{fv}}{dt} = \frac{\dot{m}_g}{\rho_p} = A_b a P_c^n \tag{8}$$

Finally, the density change in the free volume can be derived using Equations (3) and (4).

$$\frac{d\rho_c}{dt} = \frac{d\rho_c}{dP_c}\frac{dP_c}{dt} = \frac{1}{V_{fv}}\left(\dot{m}_g - \dot{m}_d - \rho_c\frac{dV_{fv}}{dt}\right) \tag{9}$$

Summarizing all the equations, three equations are used to develop the dynamic model of the VTSRM as follows:

$$\begin{aligned}\frac{dP_c}{dt} &= \frac{c^2}{V_{fv}}\left(\rho_p A_b a P_c^n - \frac{P_c A_t}{C^*} - \rho_c A_b a P_c^n\right)\\ \frac{d\rho_c}{dt} &= \frac{1}{V_{fv}}\left(\rho_p A_b a P_c^n - \frac{P_c A_t}{C^*} - \rho_c A_b a P_c^n\right)\\ \frac{dV_{fv}}{dt} &= A_b a P_c^n\end{aligned} \tag{10}$$

In Refs. [25,33], there is a validation process to confirm the dynamic model of an SRM based on the three equations (Equation (10)) compared with a cold gas experiment and CFD simulation, respectively. Through the process, we can check that it is reasonable to develop a dynamic model of an SRM based on Equation (10). Furthermore, we can also predict and analyze the performance of an SRM using Equation (10): the bigger solid propellant density (ρ_P) and the burn rate coefficient (a) and exponent (n), which are the properties of the solid propellant, the faster and bigger combustion pressure, combustion gas density, and free volume change once the combustion starts in an SRM or the nozzle throat area, which is the input variable of a VTSRM, changes.

2.3. Thrust Dynamic Modeling

The theoretical thrust of the VTSRM can be represented with the sum of the thrust by pressure difference and by momentum:

$$F = \dot{m}_d V_e + (P_e - P_a)A_e \tag{11}$$

Assuming the gas dynamics are operated under the isentropic flow and under-expansion conditions $P_e > P_a$ [34], we can represent them as:

$$V_e = \sqrt{\frac{2k}{k-1}RT\left[1 - \left(\frac{P_e}{P_c}\right)^{\frac{k-1}{k}}\right]} = M_e\sqrt{kRT\left(1 + \frac{k-1}{2}M_e^2\right)^{-1}} \tag{12}$$

$$\frac{P_e}{P_c} = \left[1 + \frac{k-1}{2}M_e^2\right]^{-\frac{k}{k-1}} \tag{13}$$

Since the nozzle exit Mach number is affected by the nozzle expansion ratio, the relation can be represented as:

$$\frac{A_e}{A_t} = \frac{1}{M_e}\left[\frac{2}{k+1}\left(1 + \frac{k-1}{2}M_e^2\right)\right]^{\frac{k+1}{2(k-1)}} \tag{14}$$

summarizing all the equations, the thrust model of a VTSRM is as follows:

$$F = \dot{m}_d M_e\sqrt{kRT\left(1 + \frac{k-1}{2}M_e^2\right)^{-1}} + \left(P_c\left[1 + \frac{k-1}{2}M_e^2\right]^{-\frac{k}{k-1}} - P_a\right)A_e \tag{15}$$

2.4. Stability Analysis

To analyze the stability of each dynamic, we linearize the system, which is composed of state equations (Equation (10)) and output equations of two dynamics (state output for

pressure dynamics and Equation (15) for thrust dynamics), under operating conditions and represent the pole-zero plot of each dynamic system, as shown in Figure 5.

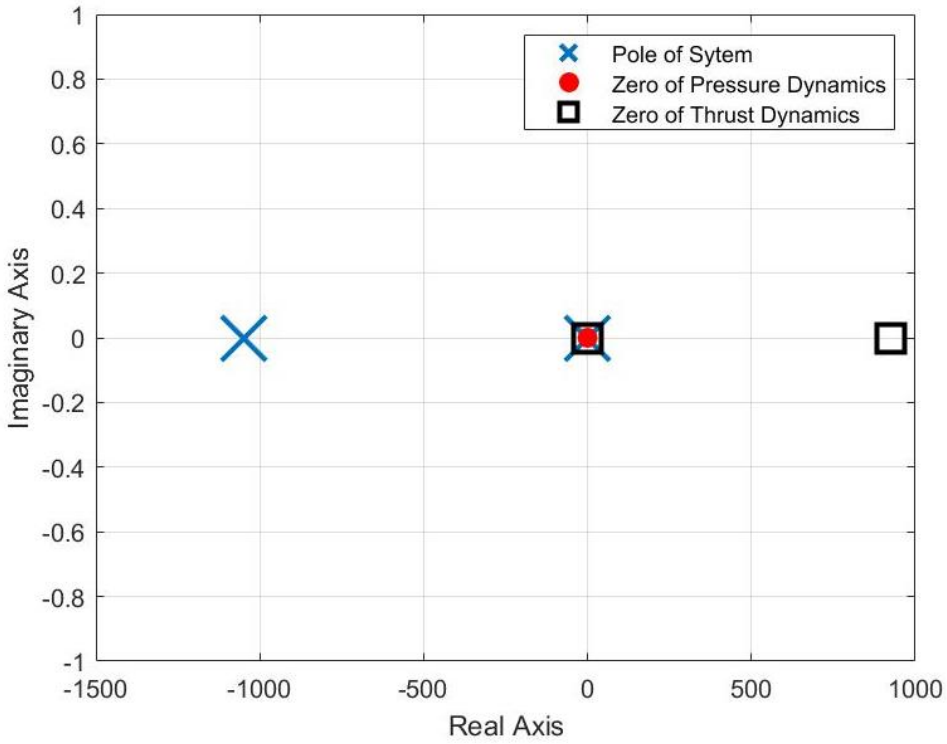

Figure 5. Pole-Zero location of the transfer function under the operating point.

In Figure 5, most poles and zeros are located close to the origin, but one pole and one zero are located on each left and right half-plane remarkably. The pole locations are the same because the systems are composed of the same state equations. However, the zero locations are different by different output equations of pressure and thrust dynamics. The poles and zeros of pressure dynamics are located on the left half of the s-plane, so the pressure dynamics is always stable. However, the pole of thrust dynamics is located on the right half of the s-plane, so the system is stable but may become unstable with undershoot when a feedback system with control is constructed. The system, which has positive zeros, calls a nonminimum phase (NMP) system and has an undershoot in the feedback system, which is a tradeoff between settling time and the undershoot size [35]. As shown in Figure 5, the thrust dynamics is an NMP system should be considered in designing a feedback system with control.

3. Pressure Control

This section deals with three types of control algorithms for pressure control: classical PID control, feedback linearization, and fuzzy PID control. To do this, we design each control algorithm and construct the feedback system, as shown in Figure 6.

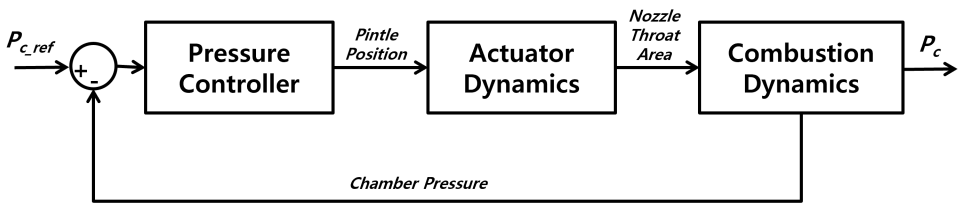

Figure 6. Schematic of pressure control.

3.1. Classical PID Control

The classical PID control algorithm is widely used in many industrial applications due to its structural simplicity and ease to design. To design classical PI control for pressure control, we linearize the nonlinear system of Equation (10) at an operating point (P_{c0}, ρ_{c0}, V_{fv0}, A_{t0}) [36].

$$\begin{aligned} \delta\dot{P}_c &= a_1\delta P_c + a_2\delta\rho_c + a_3\delta V_{fv} + a_4\delta A_t \\ \delta\dot{\rho}_c &= a_5\delta P_c + a_6\delta\rho_c + a_7\delta V_{fv} + a_8\delta A_t \\ \delta\dot{V}_{fv} &= a_9\delta P_c \end{aligned} \tag{16}$$

In Equation (16), each coefficient is $a_1 = c^2\left[(\rho_p - \rho_{c0})naA_bP_{c0}^{n-1} - A_{t0}/C^*\right]/V_{fv0}$, $a_2 = -c^2A_baP_{c0}^n/V_{fv0}$, $a_3 = -c^2\left[(\rho_p - \rho_{c0})naA_bP_{c0}^{n-1} - A_{t0}/C^*\right]/V_{fv0}^2$, $a_4 = -c^2P_{c0}/V_{fv0}C^*$, $a_5 = \left[(\rho_p - \rho_{c0})naA_bP_{c0}^{n-1} - A_{t0}/C^*\right]/V_{fv0}$, $a_6 = -A_baP_{c0}^n/V_{fv0}$, $a_7 = -\left[(\rho_p - \rho_{c0})naA_bP_{c0}^{n-1} - A_{t0}/C^*\right]/V_{fv0}^2$, $a_8 = -P_{c0}/V_{fv0}C^*$, $a_9 = A_banP_{c0}^{n-1}$.

Using Equation (16), we design the classical PI controller with a second-order linear system to simplify the time delay caused by the actuator for operating the pintle in the combustion chamber to control the nozzle throat area.

3.2. Feedback Linearization Control

The feedback linearization algorithm uses an equivalent linear system transformed from the nonlinear system through a change of variables and suitable control inputs [28]. The nonlinear dynamics of the VTSRM of Equation (10) can be expressed as:

$$\begin{bmatrix} \dot{P}_c \\ \dot{\rho}_c \\ \dot{V}_{fv} \end{bmatrix} = \begin{bmatrix} \frac{c_1P_c^n}{V_{fv}} - \frac{c_2P_c^n\rho_c}{V_{fv}} \\ \frac{c_4P_c^n}{V_{fv}} - \frac{c_5P_c^n\rho_c}{V_{fv}} \\ c_5P_c^n \end{bmatrix} + \begin{bmatrix} \frac{c_3P_c}{V_{fv}} \\ \frac{c_6P_c}{V_{fv}} \\ 0 \end{bmatrix} A_t \tag{17}$$

In Equation (17), each coefficient is $c_1 = c^2\rho_pA_ba$, $c_2 = c^2A_ba$, $c_3 = -c^2/C^*$, $c_4 = \rho_pA_ba$, $c_5 = A_ba$, $c_6 = -1/C^*$. To express the problem which tracks reference pressure P_{ref}, we use a new variable δP_c [36,37].

$$\delta P_c = P_c - P_{ref} \tag{18}$$

Since $\dot{P}_c = \delta\dot{P}_c$, we express it as:

$$\begin{bmatrix} \delta\dot{P}_c \\ \dot{\rho}_c \\ \dot{V}_{fv} \end{bmatrix} = \begin{bmatrix} \frac{c_1\left(\delta P_c+P_{ref}\right)^n}{V_{fv}} - \frac{c_2\left(\delta P_c+P_{ref}\right)^n\rho_c}{V_{fv}} \\ \frac{c_4\left(\delta P_c+P_{ref}\right)^n}{V_{fv}} - \frac{c_5\left(\delta P_c+P_{ref}\right)^n\rho_c}{V_{fv}} \\ c_5\left(\delta P_c + P_{ref}\right)^n \end{bmatrix} + \begin{bmatrix} \frac{c_3\left(\delta P_c+P_{ref}\right)}{V_{fv}} \\ \frac{c_6\left(\delta P_c+P_{ref}\right)}{V_{fv}} \\ 0 \end{bmatrix} A_t \tag{19}$$

$$\mathbf{y} = \delta P_c = h(\mathbf{x}) \tag{20}$$

In Equations (19) and (20), $\mathbf{x} = [x_1,\ x_2,\ x_3]^T = \left[\delta P_c,\ \rho_c,\ V_{fv}\right]^T$ and $\mathbf{u} = [A_t]$, so the nonlinear system has the form.

$$\begin{aligned} \dot{\mathbf{x}} &= f(\mathbf{x}) + g(\mathbf{x})\mathbf{u} \\ \mathbf{y} &= h(\mathbf{x}) \end{aligned} \tag{21}$$

To eliminate the nonlinear term of the equation, the control input variable can be expressed as:

$$A_t = \frac{V_{fv}}{c_3\left(\delta P_c + P_{ref}\right)} \times \left(-\frac{c_1\left(\delta P_c + P_{ref}\right)^n}{V_{fv}} + \frac{c_2\left(\delta P_c + P_{ref}\right)^n}{V_{fv}} + K\delta P_c + v \right) \tag{22}$$

Therefore, the propulsion dynamics can be expressed to the first-order linear ordinary differential equation as Equation (23) [28,36,37].

$$\delta \dot{P}_c = K\delta P_c + \mathbf{v} \tag{23}$$

Using the transformed combustion dynamics, we design the classical PI controller with the same actuator model in the previous session.

3.3. Fuzzy PID Control

Fuzzy control is often used as an alternative to PID control and is mainly used in the industry with the same structure as incremental PI or PID controllers [38]. This study uses the PD-Mamdani-type fuzzy controller with a PI controller for the fuzzy PID control among variable types of fuzzy PID structures [38]. The Mandani-type fuzzy controller consists of a Fuzzification, Fuzzy Inference Engine, Knowledge Base System, and Defuzzification, as shown in Figure 7.

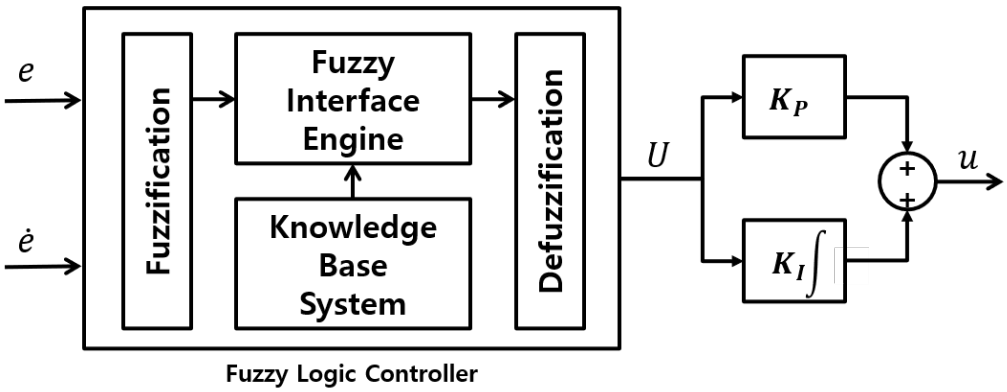

Figure 7. Fuzzy PID control structure.

The error and change in error are normalized to apply to the variable size of the step input, so they become the range [−1, 1]. The fuzzy sets for error and change in error have the Gaussian membership function as shown in Figure 8.

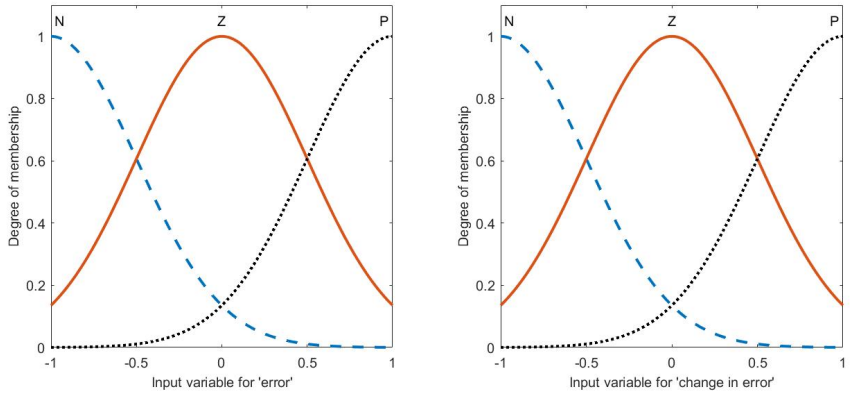

Figure 8. Fuzzy sets for fuzzy inputs in pressure control.

At defuzzification, the centroid method is generally used and is applied in this research, defined as:

$$\mathbf{z}^* = \frac{\Sigma\mu(\mathbf{z})\mathbf{z}}{\Sigma\mu(\mathbf{z})} \tag{24}$$

We obtain the output surface by the above fuzzy input sets and nine rules using Equation (24) through these processes, as shown in Figure 9. Using the fuzzy output, we choose gains by tuning with intuition and experience, mainly utilizing the gain obtained from the classical PID control design process.

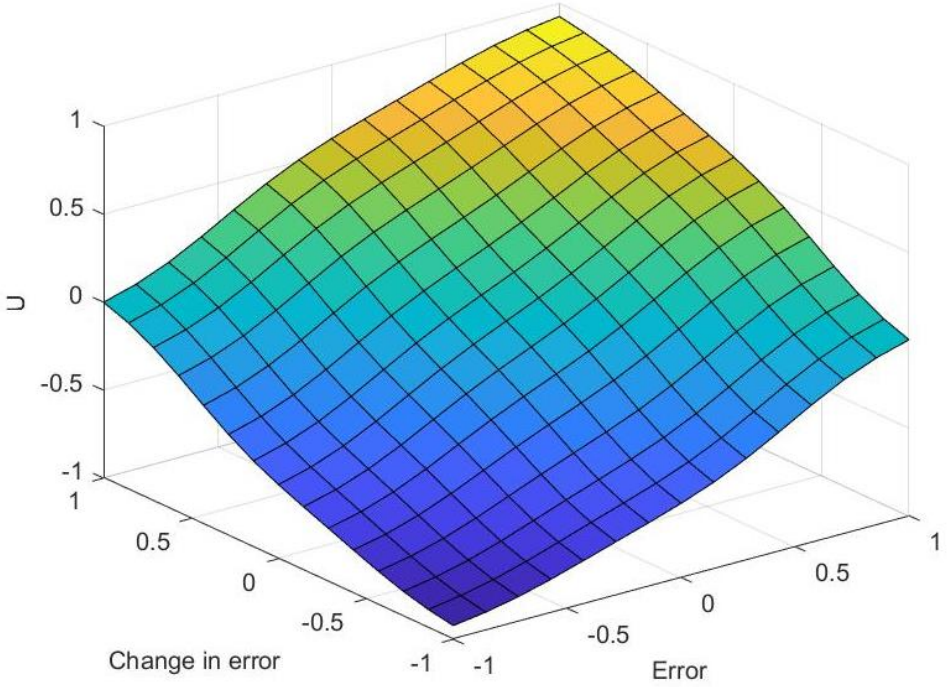

Figure 9. Control surface of outputs in pressure control.

4. Thrust Control

This section deals with control algorithms for thrust control. However, the feedback linearization algorithm cannot be applied because the trust dynamics is a biproper system by feedthrough behavior in the output equation. Therefore, we use two control algorithms which are classical PID control and fuzzy PID control. To do this, we design each control algorithm and construct the feedback system, as shown in Figure 10. Since it is hard to obtain thrust information directly in flight status, the thrust feedback control system uses an indirect method that estimates the thrust information using combustion pressure and nozzle throat area information as the dashed line in Figure 10. Generally, the Luenberger observer or Kalman filter, based on the mathematical model of the system, is used for the indirect method [39–41]. In this study, we assumed a ground test that can obtain thrust information directly by using a force sensor as the dotted line in Figure 10 to be simplified.

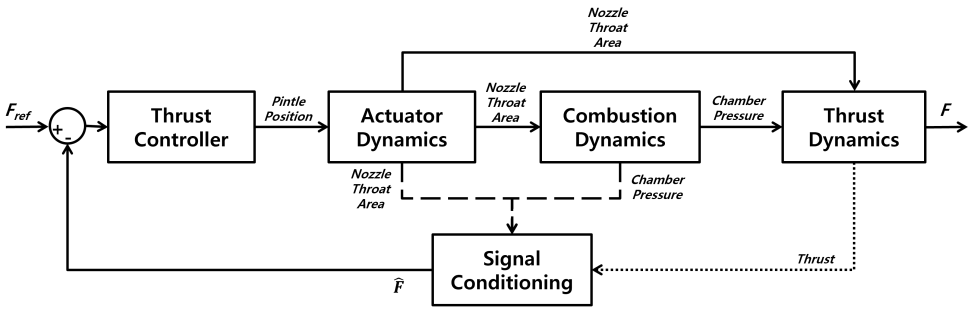

Figure 10. Schematic of thrust control.

4.1. Classical PID Control

To design classical PI control for thrust control, we linearize the Equation (11), which is the output equation under the operating point with Equation (16), which is the linearized state equation [36,37].

$$\delta F = \alpha \delta P_c + \beta \delta A_t \tag{25}$$

In Equation (25), the coefficients are $\alpha = \partial F/\partial P_c$, $\beta = \partial F/\partial A_t$. The coefficient α can be expressed as:

$$\alpha = \frac{\partial F}{\partial P_c} = \frac{\partial \dot{m}_d}{\partial P_c} V_e + \dot{m}_d \frac{\partial V_e}{\partial P_c} + \frac{\partial P_e}{\partial P_c} A_e \tag{26}$$

$$\begin{aligned} \frac{\partial \dot{m}_d}{\partial P_c} &= \frac{A_t}{C^*} \\ \frac{\partial V_e}{\partial P_c} &= \frac{1}{\sqrt{\frac{2k}{k-1} RT \left[1 - \left(\frac{P_e}{P_c}\right)^{\frac{k-1}{k}}\right]}} \frac{RT_g}{k} \left(\frac{P_e}{P_c}\right)^{\frac{k-1}{k}} \frac{1}{P_c} \\ \frac{\partial P_e}{\partial P_c} &= \left[1 + \frac{k-1}{2} M_e^2\right]^{-\frac{k}{k-1}} \end{aligned} \tag{27}$$

The coefficient β can be expressed as:

$$\begin{aligned} \beta = \frac{\partial F}{\partial A_t} &= \frac{\partial \dot{m}_d}{\partial A_t} V_e + \dot{m}_d \frac{\partial V_e}{\partial A_t} + \frac{\partial P_e}{\partial A_t} A_e \\ &= \frac{\partial \dot{m}_d}{\partial A_t} V_e + \dot{m}_d \frac{\partial V_e}{\partial M_e} \frac{\partial M_e}{\partial A_t} + \frac{\partial P_e}{\partial M_e} \frac{\partial M_e}{\partial A_t} A_e \end{aligned} \tag{28}$$

The Mach number of the nozzle exit is affected by the ratio of the nozzle exit area and nozzle throat area. However, the ratio is the function of the Mach number, the Mach number is not the function of the ratio. Therefore, we calculated the partial differential of the Mach number variation of the nozzle throat ratio variation using the implicit differentiation method [42].

$$\begin{aligned} \frac{\partial \dot{m}_d}{\partial A_t} &= \frac{P_c}{C^*} \\ \frac{\partial V_e}{\partial M_e} &= \frac{\sqrt{kRT_g}}{\left(1 + \frac{k-1}{2} M_e^2\right) \sqrt{1 + \frac{k-1}{2} M_e^2}} \\ \frac{\partial P_e}{\partial M_e} &= -kP_c M_e \left[1 + \frac{k-1}{2} M_e^2\right]^{-\frac{2k-1}{k-1}} \\ \frac{\partial M_e}{\partial A_t} &= \frac{-A_e/A_t^2}{\left[\frac{2}{k+1}\left(1 + \frac{k-1}{2} M_e^2\right)\right]^{\frac{k+1}{2(k-1)}}} \times \frac{1}{\left\{\left[\frac{2}{k+1}\left(1 + \frac{k-1}{2} M_e^2\right)\right]^{-1} - \frac{1}{M_e^2}\right\}} \end{aligned} \tag{29}$$

Using the Equations (25)–(29), we design the classical PI with the same actuator model in the previous session.

4.2. Fuzzy PID Control

The fuzzy PID control is designed using the same structure in Section 3.3. However, because of the thrust dynamics is an NMP system, as shown in Figure 5, the feedback system of the thrust dynamics may have an initial undershoot in the step response. Therefore, even the error and change in error are normalized, they would exceed 1 or -1, so the range should be more extensive than $[-1, 1]$. For this reason, the normalized error and change in error are applied in the range $[-1.5, 1.5]$, and we used different membership functions for small undershoots with fast settling, as shown in Figure 11 in this study.

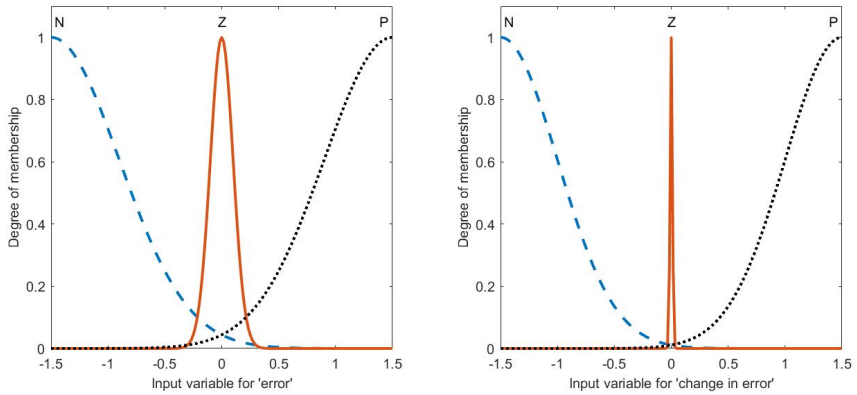

Figure 11. Fuzzy sets for fuzzy inputs in thrust control.

We obtain the output surface by the above fuzzy input sets and nine rules using Equation (24) through these processes, as shown in Figure 12. Using the fuzzy output, we choose gains in the same way with the pressure control section above.

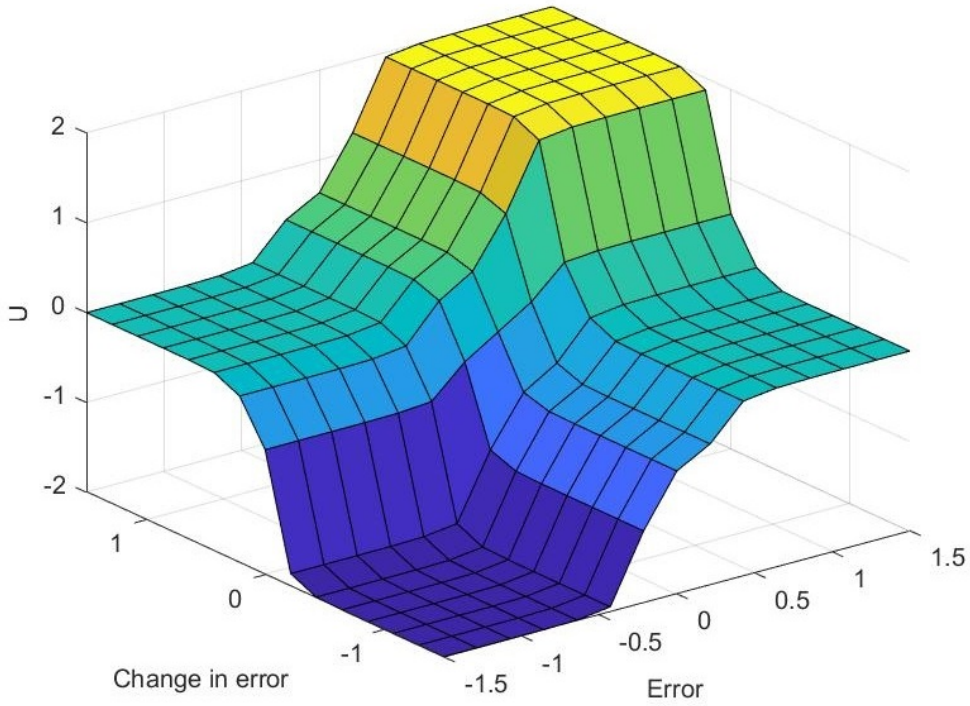

Figure 12. Control surface of outputs in thrust control.

5. Numerical Simulation and Analysis

The results of each control algorithm described in the previous sections are analyzed and compared by numerical simulation. First, we compare the three pressure controls and thrust control using the step input with variable motor dynamics. Then, we analyze the performance, including overshoot, undershoot, and settling time in the transient state caused by the step input.

5.1. Pressure Control Results and Analysis

To compare the performance of each pressure control, we analyze the performance in the transient state in step input with variable actuators. Although the time delay of the basic actuator model is 0.04 s, we apply fast (0.01 s) and slow (0.2 s) actuators to analyze under variable actuator conditions.

Figure 13 shows the performance of each pressure control algorithm with variable actuators. To compare the performance, we set the goal of the control design possessing fast settling without overshoot to be the same condition, so the settling time is a little late but does not overshoot. In the comparison results, the feedback linearization with PI control was best, and classical PID control was worst. The fuzzy PID control was between the feedback linearization and classical PID control. The performance of the fuzzy PID control is adjustable by the fuzzy sets and rules but not better than the feedback linearization without overshoot. The reason why feedback linearization has the best performance is that in the process of feedback linearization, the pressure dynamics have a simple first-order linear model, so it is easy to make a good control system.

The performance results of each control system in this study are described in Table 1. Depending on when the step input is used, the settling time changes, and overshoot can appear because of the increased free volume with time in the combustion dynamics. Therefore, the performance of control algorithms may worsen with the passing time by the characteristic change in the combustor. However, the feedback linearization control algorithm can keep the performance regardless of the time because of eliminating the nonlinearity, so the increased free volume effect is minimized in the feedback linearization process.

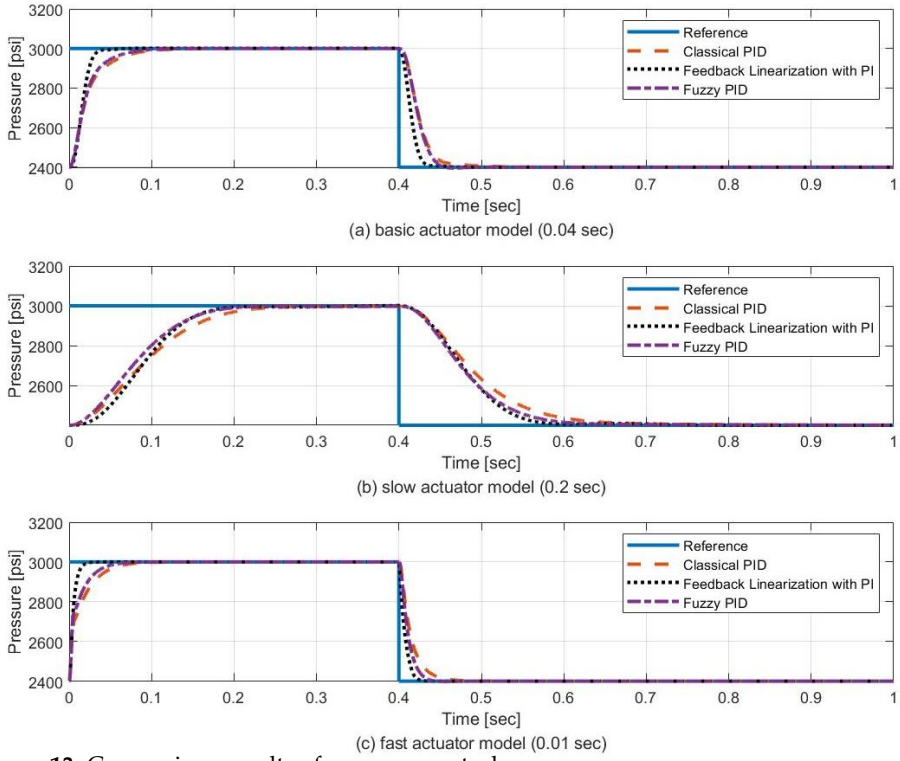

Figure 13. Comparison results of pressure control.

Table 1. Comparison results of thrust control.

Actuator	1st Settling Time			2nd Settling Time		
Model	**Classical PID**	**Feedback Linearization**	**Fuzzy PID**	**Classical PID**	**Feedback Linearization**	**Fuzzy PID**
0.01 s	0.0713	0.0183	0.0552	0.0557	0.0222	0.0339
0.04 s	0.0973	0.0362	0.0837	0.0793	0.0339	0.0488
0.2 s	0.2335	0.1866	0.1943	0.2634	0.1751	0.2084

5.2. Thrust Control and Analysis

To compare the performance of each thrust control, we analyze the performance in the same way as in the pressure control.

Figure 14 shows the performance of each thrust control algorithm with variable actuators. To compare the performance, we set the goal of the control design possessing fast settling without overshoot to be the same condition, so the settling time is a little late but not having overshoot, as in the pressure control. However, since the characteristic changes in the combustor affect the stability of the system using the classical PID control, we use input only one time in the simulation. The performance of each control system is described in Table 2. The fuzzy PID control is better for undershoot, settling time, and stability in the comparison results. Since the thrust dynamics is a biproper and NMP system, the feedback control system causes undershoot. Undershoot is an important time-domain characteristic of the response of a control system caused by several reasons [35]. There are constraints by NMP behavior which is incompatible with fast settling and small undershoot, so a tradeoff of settling and undershoot is required [35]. For this reason, the amount of undershoot changes depending on the actuator models, which are a large undershoot with the fast actuator model (settling time) and small undershoot with the slow actuator model. However, compatible with fast settling and small undershoot is feasible using the fuzzy PID control by the results. It is also possible to get better performance by tuning the fuzzy sets and control gains.

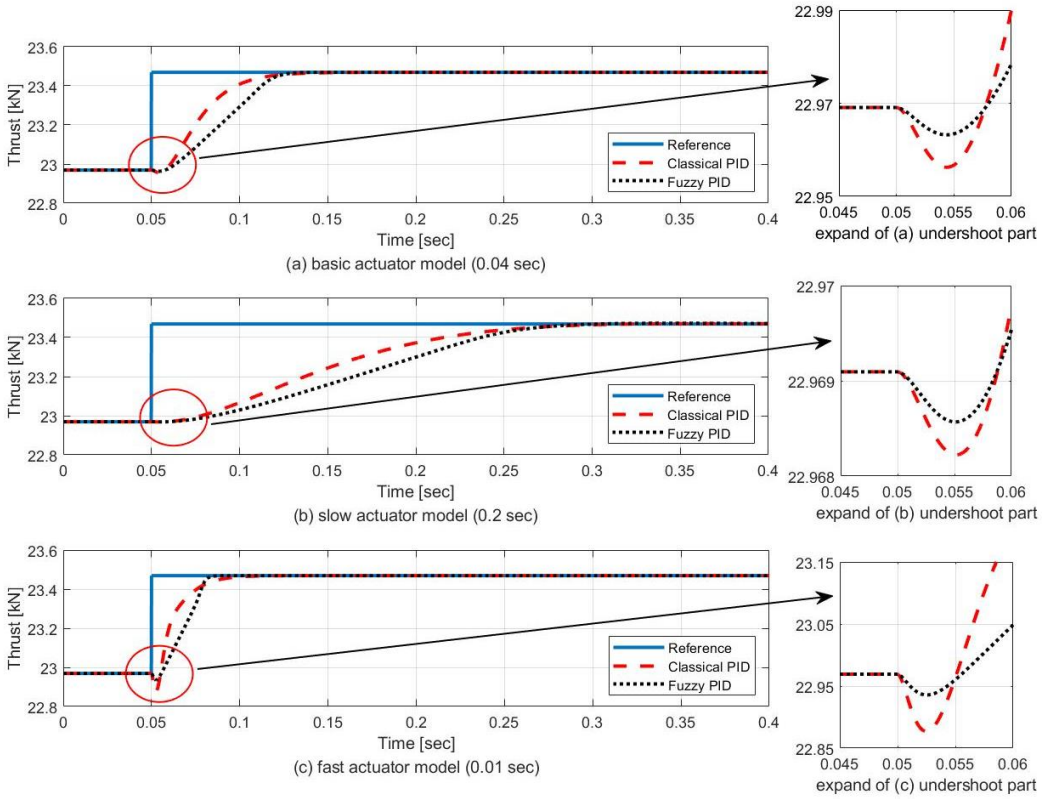

Figure 14. Comparison results of thrust control.

Table 2. Comparison results of thrust control.

Actuator Model	Undershoot		Settling Time	
	Classical PID	Fuzzy PID	Classical PID	Fuzzy PID
0.01 s	18.43 %	6.69 %	0.0954	0.0822
0.04 s	2.57 %	1.18 %	0.1267	0.1254
0.2 s	0.17 %	0.11 %	0.2825	0.2797

In terms of stability, because the characteristic change in the combustor causes instability, the closed-loop system of the NMP system with classical PID control becomes unstable after a specific input time. On the contrary, since the fuzzy PID control is one of the nonlinear control algorithms, the feedback system with the fuzzy PID control keeps stable even though the performance worsens. Therefore, the fuzzy PID control is a suitable control algorithm considering a characteristic change in the combustor of a VTSRM if a direct thrust control algorithm is used.

5.3. Combining Pressure Control and Thrust Control

Since the VTSRM is a time-variant system caused by increased free volume, the closed-loop system only using a direct thrust control becomes an unstable system easily after a specific time. Therefore, we use two control steps combining pressure control and thrust control to construct a stable system, as shown in Figure 15. In the closed-loop system with combined control, the variables, including the increased free volume, are made stable by pressure control and thrust control. The control algorithms of the combined control are used, which are dealt with in the previous sections, and we compare the performance of each combination. As described in the thrust control section, we assumed a ground test that can obtain thrust information directly with a force sensor as in the dotted line in Figure 15.

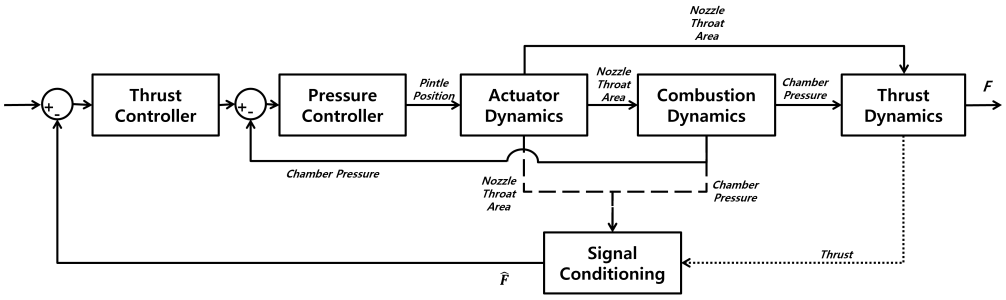

Figure 15. Schematic of thrust control with pressure control.

Figures 16 and 17 show the performance of each combining control with the basic actuator (0.04 s). Since the performance of the system changes by the increased free volume in the combustor with time, the goal of design is not to have overshoot in the first transient state, so the overshoot appears in the second transient state. The performance of each control system with the tuned control gains in previous sections is described in Table 3. Since the thrust control is performed after the state variables of the system become stable by pressure control, the closed-loop system with the combining control is always stable, regardless of which control algorithms it is combined with. Therefore, combining thrust and pressure control is a reasonable control considering a characteristic change in the combustor of a VTSRM to be more stable. Considering settling time and undershoot in the first transient state, combining fuzzy PID control and feedback linearization is best in the first transient state. However, as time goes by, the performance of each combining control is changed, so the best control is varied with the operating time and way of VTSRM. In this study, we tune gains with the same fuzzy set and control surface described in the previous section. Therefore, using the adaptive fuzzy set and control surface, combining control with fuzzy PID control will be more effective in controlling VTSRM.

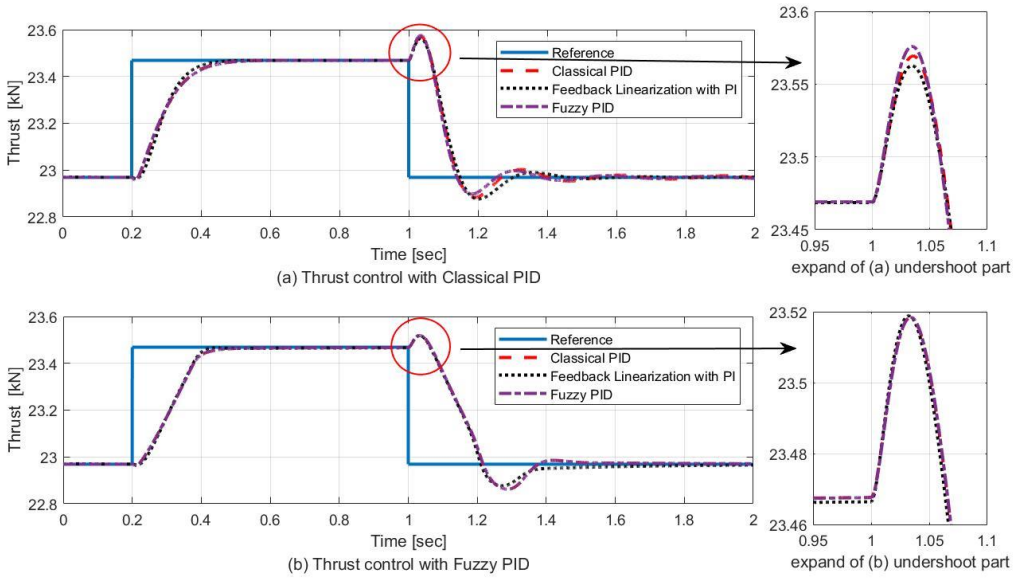

Figure 16. Comparison thrust results of combining control.

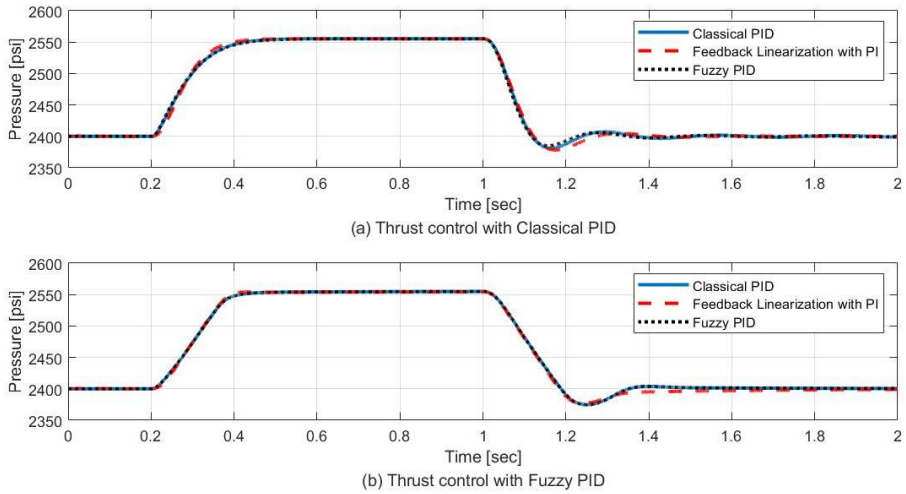

Figure 17. Comparison pressure results of combining control.

Table 3. Comparison results of thrust control with pressure control.

Thrust Control	Pressure Control	1st Transient		2nd Transient		
		Undershoot	Settling Time	Undershoot	Overshoot	Settling Time
Classical PID	Classical PID	1.98%	0.2647	20.05%	17.17%	0.505
	Feedback Linearization	1.13%	0.2319	18.71%	18.42%	0.417
	Fuzzy PID	2.16%	0.2759	21.36%	14.27 %	0.465
Fuzzy PID	Classical PID	1.10%	0.2561	9.85 %	21.37%	0.474
	Feedback Linearization	0.63%	0.2130	9.95%	18.50%	0.625
	Fuzzy PID	1.11%	0.2561	9.88%	21.39%	0.476

6. Conclusions

This paper deals with pressure and thrust control for a variable-thrust solid-propellant rocket motor (VTSRM), considering characteristic changes in the combustor and performance comparison of each control algorithm. To confirm and compare the performance of pressure and thrust control algorithms, we develop a dynamic simulation model of a VTSRM with a pintle nozzle to control the pressure and thrust, then design control systems, finally comparing the performance of each control algorithm. Through this study, since the pressure dynamics of the VTSRM is a strictly proper system, the characteristic changes in the combustor do not affect the stability of the pressure control system. However, on the contrary, because thrust dynamics is a biproper system and nonminimum phase (NMP) system, the characteristic changes affect the stability of the thrust control system directly if not using a nonlinear control algorithm. Furthermore, the thrust control system using a fuzzy PID control can have a fast settling time with a small undershoot even if the dynamics are a nonminimum phase (NMP) system, requiring a tradeoff settling time and undershoots [35]. Finally, we show that a combining pressure and thrust control is always stable even though the characteristic changes in the combustor make an unstable system.

Author Contributions: Conceptualization, J.C. and É.J.d.O.; methodology, J.C. and É.J.d.O.; software, J.C.; validation, J.C.; resources, J.C.; preparation of the initial draft, J.C. and É.J.d.O.; modifications and revisions, J.C. and É.J.d.O. All authors have read and agreed to the published version of the manuscript.

Funding: This research received no external funding.

Institutional Review Board Statement: Not applicable.

Informed Consent Statement: Not applicable.

Data Availability Statement: Not applicable.

Conflicts of Interest: The authors declare no conflict of interest.

Abbreviations

The following abbreviations are used in this manuscript:

A_b	Burning surface area
A_e	Nozzle exit area
A_t	Nozzle throat area
C^*	Characteristic velocity
F	Thrust
M	Accumulated mass in the free volume
M_e	Nozzle exit Mach number
P_a	Ambient pressure
P_c	Combustion chamber pressure
P_e	Nozzle exit pressure
R	Combustion gas constant
T	Combustion chamber temperature
V_{fv}	Free volume of chamber
V_e	Nozzle exit velocity
a	Burn rate coefficient
c	Speed of sound of combustion gas
k	Specific heat ratio
$\dot{m}_d$	Discharge mass flow rate from chamber
$\dot{m}_g$	Generated mass flow rate from solid propellant
n	Burn rate exponent
ρ_c	Combustion gas density
ρ_p	Solid propellant density

References

1. Sutton, G.P.; Biblarz, O. *Rocket Propulsion Elements*, 9th ed.; John Wiley & Sons: Hoboken, NJ, USA, 2016.
2. Mahjub, A.; Mazlan, N.M.; Abdullah, M.Z.; Azam, Q. Design Optimization of Solid Rocket Propulsion: A Survey of Recent Advancements. *J. Spacecr Rockets* **2020**, *57*, 3–11. [CrossRef]
3. Hernandez, R.N.; Singh, H.; Messimer, S.L.; Patterson, A.E. Design and performance of modular 3-D printed solid-propellant rocket airframes. *Aerospace* **2017**, *4*, 17. [CrossRef]
4. Tummala, A.R.; Dutta, A. An overview of cube-satellite propulsion technologies and trends. *Aerospace* **2017**, *4*, 58. [CrossRef]
5. Da Cás, P.L.; Veras, C.A.; Shynkarenko, O.; Leonardi, R. A Brazilian space launch system for the small satellite market. *Aerospace* **2019**, *6*, 123. [CrossRef]
6. McDonald, A. Solid rockets-An affordable solution to future space propulsion needs. In Proceedings of the 20th Joint Propulsion Conference, Cincinnati, OH, USA, 11–13 June 1984.
7. Caubet, P.; Berdoyes, M. Innovative ArianeGroup Controllable Solid Propulsion Technologies. In Proceedings of the AIAA Propulsion and Energy 2019 Forum, Indianapolis, IN, USA, 19–22 August 2019.
8. Alan, A.; Yildiz, Y.; Poyraz, U. Adaptive pressure control experiment: Controller design and implementation. In Proceedings of the 2017 IEEE Conference on Control Technology and Applications (CCTA), Kohala Coast, HI, USA, 27–30 August 2017.
9. Yonggang, G.; Yang, L.; Zexin, C.; Xiaocong, L.; Chunbo, H.; Xiaojing, Y. Influence of lobe geometry on mixing and heat release characteristics of solid fuel rocket scramjet combustor. *Acta Astronaut.* **2019**, *164*, 212–229. [CrossRef]
10. Yang, L.; Yonggang, G.; Lei, S.; Zexin, C.; Xiaojing, Y. Preliminary experimental study on solid rocket fuel gas scramjet. *Acta Astronaut.* **2018**, *153*, 146–153. [CrossRef]
11. Chang, J.; Li, B.; Bao, W.; Niu, W.; Yu, D. Thrust control system design of ducted rockets. *Acta Astronaut.* **2011**, *69*, 86–95. [CrossRef]
12. Ponti, F.; Mini, S.; Fadigati, L.; Ravaglioli, V.; Annovazzi, A.; Garreffa, V. Effects of inclusions on the performance of a solid rocket motor. *Acta Astronaut.* **2021**, *189*, 283–297. [CrossRef]
13. Alan, A.; Yildiz, Y.; Poyraz, U. High-performance adaptive pressure control in the presence of time delays: Pressure control for use in variable-thrust rocket development. *IEEE Contr. Syst. Mag.* **2018**, *38*, 26–62. [CrossRef]
14. Bergmans, J.; Di Salvo, R. Solid Rocket Motor Control: Theoretical Motivation and Experimental Demonstration. In Proceedings of the 39th AIAA/ASME/SAE/ASEE Joint Propulsion Conference and Exhibit, Huntsville, AL, USA, 20–23 July 2003.
15. Lee, H.S.; Lee, D.Y.; Park, J.S.; Kim, J.K. A Study on Pressure Control for Variable Thrust Solid Propulsion System Using Cold Gas Test Equipment. *J. Korean Soc. Aeronaut.* **2009**, *37*, 76–81.
16. Hong, S. Gain Scheduling Controller Design and Performance Evaluation for Thrust Control of Variable Thrust Solid Rocket Motor. *J. Korean Soc. Aeronaut.* **2016**, *20*, 28–36.
17. Napior, J.; Garmy, V. Controllable solid propulsion for launch vehicle and spacecraft application. In Proceedings of the 57th International Astronautical Congress, Valencia, Spain, 2–6 October 2006.
18. Lim, Y.; Lee, W.; Bang, H.; Lee, H. Thrust distribution for attitude control in a variable thrust propulsion system with four ACS nozzles. *Adv. Space Res.* **2017**, *59*, 1848–1860. [CrossRef]
19. Lee, H.; Bang, H. Efficient Thrust Management Algorithm for Variable Thrust Solid Propulsion System with Multi-Nozzles. *J. Spacecr Rockets.* **2020**, *57*, 328–345. [CrossRef]
20. Ji, M.; Chang, H. Modeling and dynamic characteristics analysis on solid attitude control motor using pintle thrusters. *Aerosp. Sci. Technol.* **2020**, *106*, 106130.
21. Saravanan, V.; Ko, J.; Lee, S.; Murugan, N.; Kumar, V.S. Conceptual aerodynamic design of pintle nozzle for variable-thrust propulsion. *Int. J. Aeronaut. Space Sci.* **2020**, *21*, 1–14. [CrossRef]
22. Song, A.; Wangm, N.; Li, J.; Ma, B.; Chen, X. Transient flow characteristics and performance of a solid rocket motor with a pintle valve. *Chin. J. Aeronaut.* **2020**, *33*, 3189–3205. [CrossRef]
23. Sapkota, J.; Xu, Y.H.; Sun, H.J. Numerical Study on Response Characteristics of Solid Rocket Pintle Motor. *J. Aerosp. Technol. Manag.* **2019**, *11*. [CrossRef]
24. Yan, D.; Wei, Z.; Xie, K.; Wang, N. Simulation of thrust control by fluidic injection and pintle in a solid rocket motor. *Aerosp. Sci. Technol.* **2020**, *99*, 105711. [CrossRef]
25. Ko, H.; Lee, J. Cold tests and the dynamic characteristics of the pintle type solid rocket motor. In Proceedings of the 49th AIAA/ASME/SAE/ASEE Joint Propulsion Conference, San Jose, CA, USA, 14–17 July 2013.
26. Naumann, K.W.; Hopfe, N. Hot Gas Nozzle-Valve Assembly and Control Method for Continuously Operating Divert-and Attitude Control Systems. In Proceedings of the AIAA Propulsion and Energy 2019 Forum, Indianapolis, IN, USA, 19–22 August 2019.
27. Martins, L.; Cardeira, C.; Oliveira, P. Feedback linearization with zero dynamics stabilization for quadrotor control. *J. Intell. Robot. Syst.* **2021**, *101*, 1–17. [CrossRef]
28. Khalil, H.K. *Nonlinear Systems*, 1st ed.; Prentice Hall: Upper Saddle River, NJ, USA, 2002.
29. Piltan, F.; Yarmahmoudi, M.; Mirzaie, M.; Emamzadeh, S.; Hivand, Z. Design novel fuzzy robust feedback linearization control with application to robot manipulator. *Int. J. Intell. Syst. Appl.* **2013**, *5*, 1. [CrossRef]
30. Li, E.H.; Li, Y.Z.; Li, J.X.; Lou, Y.Y. An investigation on fuzzy incremental control strategy of water membrane evaporator cooling loop for mars spacesuit. *Acta Astronaut.* **2021**, *182*, 66–76. [CrossRef]

31. Chak, Y.C.; Varatharajoo, R.; Razoumny, Y. Disturbance observer-based fuzzy control for flexible spacecraft combined attitude & sun tracking system. *Acta Astronaut.* **2017**, *133*, 302–310.
32. Hu, Y.; Yang, Y.; Li, S.; Zhou, Y. Fuzzy controller design of micro-unmanned helicopter relying on improved genetic optimization algorithm. *Aerosp. Sci. Technol.* **2020**, *98*, 105685. [CrossRef]
33. Lee, J. A Study on the Static and Dynamic Characteristics of Pintle-Perturbed Conical Nozzle Flows. Ph.D. Thesis, Department of Mechanical Engineering, Yonsei University, Seoul, Korea, 2012.
34. Mattingly, J.D. *Elements of Gas Turbine Propulsion*, 1st ed.; McGraw-Hill: New York, NY, USA, 1996.
35. Lau, K.; Middleton, R.H.; Braslavsky, J.H. Undershoot and settling time tradeoffs for nonminimum phase systems. *IEEE Trans. Automat. Contr.* **2003**, *48*, 1389–1393. [CrossRef]
36. Cha, J.; Ko, S.; Suh, S. Control of Pressure and Thrust for a Variable Thrust Solid Propulsion System Using Linearization Considering Characteristic Changes in the Combustor. In Proceedings of the 2013 KSPE Spring Conference, Busan, Korea, 29–31 May 2013.
37. Kim, Y.; Cha, J.; Ko, S.; Kim, D. Control of pressure and thrust for a variable thrust solid propulsion system using linearization. *J. KSPE* **2011**, *15*, 18–25.
38. Yesil, E.; Guzelkaya, M.; Eksin, I. Fuzzy PID controllers: An overview. In Proceedings of the 3rd Triennial ETAI International Conference on Applied Automatic Systems, Skopje, North Macedonia, 18–20 September 2003.
39. Henriksson, M.; Grönstedt, T.; Breitholtz, C. Model-based on-board turbofan thrust estimation. *Control Eng. Pract.* **2011**, *19*, 602–610. [CrossRef]
40. Ring, D.; Henriksson, M. Thrust control for a turbofan engine using estimation. In Proceedings of the Turbo Expo: Power for Land, Sea, and Air, Barcelona, Spain, 8–11 May 2006.
41. Zhang, Y.; Zhao, Z.; Lu, T.; Yuan, L.; Xu, W.; Zhu, J. A comparative study of Luenberger observer, sliding mode observer and extended Kalman filter for sensorless vector control of induction motor drives. In Proceedings of the 2009 IEEE Energy Conversion Congress and Exposition, San Jose, CA, USA, 20–24 September 2009.
42. Cha, J. A Study on Thrust Control System Design for Multi-Nozzle Solid Propulsion System. Master's Thesis, Department of Aerospace and Mechanical Engineering, Korea Aerospace University, Goyang, Korea, 2014.